Human Family with Sequence Similarity 60 Member A (FAM60A) Protein: a New Subunit of the Sin3 Deacetylase Complex*[S]

Karen T. Smith‡, Mihaela E. Sardiu‡, Skylar A. Martin-Brown‡‖, Chris Seidel‡, Arcady Mushegian‡§, Rhonda Egidy‡, Laurence Florens‡, Michael P. Washburn‡¶, and Jerry L. Workman‡**

Here we describe the function of a previously uncharacterized protein, named *fam*ily with sequence similarity *60* member *A* (FAM60A) that maps to chromosome 12p11 in humans. We use quantitative proteomics to determine that the main biochemical partners of FAM60A are subunits of the Sin3 deacetylase complex and show that FAM60A resides in active HDAC complexes. In addition, we conduct gene expression pathway analysis and find that FAM60A regulates expression of genes that encode components of the TGF-beta signaling pathway. Moreover, our studies reveal that loss of FAM60A or another component of the Sin3 complex, SDS3, leads to a change in cell morphology and an increase in cell migration. These studies reveal the function of a previously uncharacterized protein and implicate the Sin3 complex in suppressing cell migration. ***Molecular & Cellular Proteomics 11: 10.1074/mcp.M112.020255, 1815–1828, 2012.***

Histone deacetylases (HDACs)[1] catalyze the removal of acetyl groups from proteins. Histones may be the main targets of these enzymes, but they also mediate deacetylation of many nonhistone proteins (1). There are 11 human histone deacetylases and these fall into four different classes, three of which (Classes I, II, IV) belong to a large superfamily of zinc-dependent deacetylases, and the fourth (Class III, or Sirtuins) are NAD+ dependent (2–4). Of the HDACs, those in Class I (HDACs 1, 2 and 3) are known to reside in large multisubunit complexes that help to specify and diversify HDAC function (3).

From the ‡Stowers Institute for Medical Research, Kansas City, Missouri 64110, USA; §Department of Microbiology, Molecular Genetics, and Immunology, University of Kansas Medical Center, Kansas City, KS 66160, USA; ¶Department of Pathology and Laboratory Medicine, University of Kansas Medical Center, Kansas City, Kansas 66160, USA

Received May 2, 2012, and in revised form, August 9, 2012
Published, MCP Papers in Press, September 14, 2012, DOI 10.1074/mcp.M112.020255

[1] The abbreviations used are: HDAC, histone deacetylases; ChIP, chromatin immunoprecipitation; MudPIT, multidimensional protein identification technology; AP-MS, affinity purification followed by mass spectrometry.

HDACs 1 and 2 are found together in at least three distinct protein complexes, Mi-2/Nurd, CoREST and Sin3 (3). The Sin3/HDAC complex can affect cell cycle progression through multiple mechanisms (5–8). Different subunits of Sin3 contribute to different functions. For example, SDS3 is a core component within the Sin3 complex necessary to hold the complex together and important for catalytic activity (9, 10). Other protein subunits are not needed for the integrity of the Sin3 complex and appear to have more peripheral functions. They may mediate interactions with chromatin or sequence specific transcription factors. For example, *in*hibitor of *g*rowth *1* and *2* (ING1 and ING2), tether the complex to specific marks on chromatin (11).

Other subunits, such as Sin3, can recruit the complex to different subsets of genes, through interactions with specific transcription factors (12–14). Therefore the Sin3 complex has diverse effects on biological processes that are mediated through distinct subunits.

Importantly, the Sin3 complex is among the targets of anticancer drugs called HDAC inhibitors (15). These drugs work through a number of different cellular mechanisms (16). Biochemically, they bind to the catalytic sites of HDACs and therefore it is assumed that they completely abrogate all of their functions. However, it appears that these drugs may preferentially target some of the noncatalytic subunits of these HDAC complexes (15, 17). This is particularly important to understand because not all subunits of the Sin3 complex appear to be cancer promoting. For example, *br*east cancer *m*etastasis *s*uppressor *1* (BRMS1) can suppress metastasis of cancer in mouse models (18). In addition, ING1 and *r*etinoblastoma *b*inding *p*rotein *1* (RBP1) display tumor suppressive properties (19, 20). Moreover, some Sin3 complex subunits may display both tumor suppressive and oncogenic properties depending on the context (*i.e.* ING2) (21, 22). Therefore it is important to understand the complete set of functions encoded by this complex, which subunits mediate these functions and how they are affected by HDAC inhibitors.

In this study, we present a systematic quantitative AP-MS analysis of the Sin3/HDAC complex by utilizing multidimen-

sional protein identification technology (MudPIT) and discovered a novel subunit of the Sin3 complex, named FAM60A. This protein lacks homology to other proteins in the human proteome, but is conserved in metazoans. To demonstrate a consistent recovery of FAM60A we examined the complex around six bait proteins. In all, FAM60A was reproducibly detected with high relative abundance values. Reciprocal analysis of FAM60A protein demonstrated a strong association with all selected subunits of the Sin3/HDAC complex. Subsequently, through a series of biochemical approaches and microarray analysis we were able to reveal novel insights into the function of FAM60A protein.

Interestingly, we discover that FAM60A represses genes in the TGF-beta signaling pathway. We show that these gene expression changes are linked to FAM60A's role in the Sin3 complex, as SDS3 knockdowns have similar gene expression profiles. Additionally, we find that loss of FAM60A leads to a change in cell morphology and an increase in cell migration in lung cancer and liver cancer cells. These effects are dependent on signaling through the TGF-beta receptors 1 and 2. Importantly, when the SDS3 subunit of the Sin3 complex is abrogated, cells also undergo a change in morphology and an increase in migration. The data suggest that the functions of FAM60A revealed in this study are linked to its occupancy in Sin3. Overall, this work reveals that FAM60A functions in the Sin3 complex as a repressor of TGF-beta signaling and cell migration.

EXPERIMENTAL PROCEDURES

Cell Lines and Culture—293T cells stably expressing FAM60A-FLAG were produced using the Flp-In system (Invitrogen). Cells were maintained in Dulbecco's modified Eagle's medium (GIBCO) supplemented with 10% fetal bovine serum (FBS). A549 cells were obtained from the American Type Culture Collection (ATCC) and maintained in F-12K media (Cellgro) with 10% FBS. Both cell lines were grown at 37% degrees with 5% CO_2 in a humidified atmosphere. Additional cancer cell line lysates were obtained from Aviva Systems Biology or Protein Biotechnologies.

Plasmids—Full length cDNA encoding human FAM60A (NCBI Reference Sequence: NM_021238.2) was cloned into pcDNA5-FRT with a single C-terminal FLAG tag.

Biochemical Purifications—293T whole cell extracts were made as previously described (Mahrour, 2008). Nuclear extracts were made according to Dignam (23). FLAG purifications from 293T cells were carried out overnight at 4°C using anti-FLAG M2 resin (Sigma). FLAG beads were washed four times for 10 mins each with rotation at 4 °C. Sixty volumes of wash buffer to bead volume were used per wash with the following buffer: 10 mM HEPES pH 7.5, 0.2% Triton X-100, 0.3 M NaCl, 10 mM KCl, and 1.5 mM $MgCl_2$. After washing, proteins were eluted using 3× FLAG peptide (Sigma) diluted to a concentration of 0.2 mg/ml in a buffer containing 50 mM Tris pH 7.5, 0.5% Nonidet P-40, and 0.3 M NaCl. Complexes were then analyzed by MudPIT, silver staining or used in HDAC assays.

MudPIT Mass Spectrometry and Database Searching—

Preparation of Peptide Mixtures—TCA-precipitated protein samples from ING2, SAP30, SAP30L, HDAC1, BRMS1, and BRMS1L Flag-IPs were solubilized in 30 μl of freshly made 0.1 M Tris-HCl, pH 8.5, 8 M urea, 5 mM TCEP (Tris(2-Carboxylethyl)-Phosphine Hydrochloride, Pierce). After 30 min at room temperature, freshly made 0.5 M IAM (Iodoacetamide, Sigma) was added to a final concentration of 10 mM, and the samples were left at room temperature for another 30 min in the dark. Endoproteinase Lys-C (Roche) was first added at an estimated 1:100 (wt/wt) enzyme to protein ratio, for at least 6 h at 37 °C. Urea was then diluted to 2 M with 0.1 M Tris-HCl, pH 8.5, $CaCl_2$ was added to 0.5 mM, and modified trypsin (Promega), 1:100 (wt/wt), was added for over 12 h at 37 °C. All enzymatic digestions were quenched by adding formic acid to 5%.

Data Acquisition—Each trypsin-digested sample was analyzed independently by Multidimensional Protein Identification Technology (MudPIT) as described previously (24, 25).

Peptide mixtures were pressure-loaded onto a 100 μm fused-silica column pulled to a 5 μm tip using a P 2000 CO_2 laser puller (Sutter Instruments). The microcapillary columns were packed first with 8 cm of 5 μm C18 reverse phase (RP) particles (Aqua, Phenomenex), followed by 3 cm of 5 μm strong cation exchange material (Partisphere SCX, Whatman), and by 2 cm of RP particles (26). Loaded microcapillaries were placed in line with LTQ ion trap mass spectrometers (ThermoScientific, San Jose, CA) interfaced with quaternary Agilent 1100 quaternary pumps (Agilent Technologies, Palo Alto, CA). Overflow tubing was used to decrease the flow rate from 0.1 ml/min to about 200–300 nl/min. During the course of a fully automated chromatography, ten 120-min cycles of increasing salt concentrations followed by organic gradients slowly released peptides directly into the mass spectrometer (27). Three different elution buffers were used: 5% acetonitrile, 0.1% formic acid (Buffer A); 80% acetonitrile, 0.1% formic acid (Buffer B); and 0.5 M ammonium acetate, 5% acetonitrile, 0.1% formic acid (Buffer C). The last two chromatography steps consisted of a high salt wash with 100% Buffer C followed by the acetonitrile gradient. The application of a 2.5 kV distal voltage electrosprayed the eluting peptides directly into LTQ linear ion trap mass spectrometers equipped with a nano-LC electrospray ionization source (ThermoFinnigan). Each full MS scan (from 400 to 1600m/z) was followed by five MS/MS events using data-dependent acquisition where the 1st most intense ion was isolated and fragmented by collision-induced dissociation (at 35% collision energy), followed by the 2nd to 5th most intense ions.

Data Analysis—RAW files were converted to the ms2 format using RAWDistiller v. 1.0, an in-house developed software. The ms2 files were subjected to database searching using SEQUEST (version 27 (rev.9)) with no enzyme specificity considered (28). The mass tolerance for precursor ions was set at 3 amu, whereas the mass tolerance for fragment ions was 0 amu. MS/MS spectra were searched against a protein database consisting of 29375 nonredundant human proteins (NCBI, 2010-11-22 release) and 160 sequences for usual contaminants (such as keratins, proteolytic enzymes, etc. In addition, to estimate false discovery rates, each nonredundant protein entry was randomized. The resulting "SHUFFLED" sequences were added to the database and searched at the same time as the "forward" sequences. To account for carboxamidomethylation by IAM, +57 Da was added statically to cysteine residues and +16 Da for oxidized methionine residues for all the searches. Results from different runs were compared and merged using CONTRAST (29). Spectrum/peptide matches were only retained if peptides were at least seven amino acids long and were fully tryptic. The DeltCn had to be at least 0.08, with minimum XCorrs of 1.8 for singly, 2.0 for doubly, and 3.0 for triply charged spectra, and a maximum Sp rank of 10. Finally, combining all runs, proteins had to be detected by at least two such peptides, or one peptide with two independent spectra. Proteins that were subset of others were removed.

Quantitation was performed using label-free spectral counting. The number of spectra identified for each protein was used for calculating the distributed normalized spectral abundance factors (dNSAF) (30). *NSAF v7* (an in-house developed software) was used to create the

final report on all nonredundant proteins detected across the different runs, estimate false discovery rates (FDR), and calculate their respective distributed Normalized Spectral Abundance Factor (dNSAF) values. Under these criteria the spectral FDRs ranged from 0.00–0.436%, the peptide FDRs ranged from 0.00–0.868% and the protein FDRs ranged from 0.000–2.838% respectively for all pull-downs. Protein-protein interaction networks were created using Cytoscape software (31).

HDAC Assays—HDAC assays were performed as described previously (15). Where indicated, trichostatin A was added at a concentration of 1 μm to the assay.

Antibodies—Antiserum against human FAM60A was raised in New Zealand White rabbits (Covance), to the following peptide: SSSRFTDSKRYE. The following commercially available antibodies were used: FLAG-HRP (Sigma); Beta-tubulin, Mab380 (Upstate/Millipore); E-cadherin, Ab53033 (Abcam, Cambridge, MA); SDS3, A300–235A (Bethyl Laboratories, Montgomery, TX); ING2, 11560–11561-AP (ProteinTech Group, Inc.).

siRNA Transfections—A549 cells were plated at ~20% confluency the day prior to transfections. Cells were transfected using Dharmafect 1 (Dharmacon) and 50 nM siRNAs (Ambion). Ambion siRNA ID #s are as follows: Control siRNA (AM4637); FAM60A siRNA #1 (s33909); FAM60A siRNA #2 (147804); FAM60A siRNA #3 (s33911); ING2 siRNA (116981); SDS3 siRNA (s34742).

Migration Assays and Microscopy—Migration assays were carried out in one of two different formats. A. Cells were plated in 6-well plates and transfected 1 day after plating. Scratches were made using a p10 pipette tip when cells reached near confluency. Lines were drawn on the underside of the tissue culture plates to orient scratches and ensure the same region was monitored each day. After scratching, cells were washed, and serum was reduced in the media to 0.5%. B. Alternatively, RADIUS cell migration assays were used (Catalog # CBA-125, Cell Biolabs, Inc.). Cells were transfected 1 day after plating and drugs were added where appropriate 1 day after transfection. Two days (A549s) or 3 days (HepG2s) after transfection, when cells were confluent, the RADIUS gel spot was removed according to the manufacturer's protocol in order to simulate a wound. Media was changed to 0.5% serum and drugs were added during media changes as necessary. Scratches/wounds for all assays were monitored daily. Pictures were taken of the starting scratches/wounds and each day post-scratch, using an Axiovert 200 inverted widefield microscope (Carl Zeiss). Areas were measured by using the "outline" function on the Axiovision program (release 4.7.2). Percent closure was calculated by subtracting the open area over time, from the original starting open area. To minimize variation because of different starting wound sizes, wounds for A549 cells were only considered if they were within $\pm$12% of the average starting scratch/wound size for that experiment. Migration assays were performed on at least three independent transfections for each siRNA.

BrdU Incorporation Assays—A549 or HepG2 cells were transfected with control siRNAs or siRNAs against FAM60A. Three days after transfection, cells were incubated for 5 hours (A549) or 20 hours (HepG2) with BrdU. BrdU incorporation was detecting using the BrdU and Ki67 cell proliferation kit (Cellomics) according to manufacturer's protocol. Cells were costained with DAPI. Percent incorporation of BrdU in each well was measured by fluorescence analysis using a Celigo Adherent Cell Cytometer (Cyntellect). Data from at least three independent transfections for each siRNA were obtained.

Microarrays—RNA was extracted from A549 cells 3 days post-transfection. RNAs from three independent transfections for each siRNA were used. RNA was purified using TRIzol (Invitrogen), and run through an RNeasy clean up column (Qiagen). Concentration and quality of RNA were determined by spectrophotometer and Agilent bioanalyzer analysis (Agilent Technologies, Inc., Palo Alto, CA). For array analysis, labeled mRNA (aRNA) targets were prepared from 1 μg of total RNA using the MessageAmp II-Biotin Enhanced RNA Amplification kit (Applied Biosystems/Ambion, Austin, TX) according to the manufacturer's specifications. Array analysis was performed using Affymetrix GeneChip Human Genome U133 Plus 2.0 Arrays processed with the GeneChip Fluidics Station 450 and scanned with a GeneChip Scanner 3000 7G using standard protocols. Affymetrix CEL files were processed in the R statistical environment and normalized using RMA (32). The linear modeling package Limma (33), was used to derive gene expression coefficients and calculate p values. p Values were adjusted for multiple hypothesis testing using the method of Benjamini and Hochberg (34). The data have been deposited in GEO with accession number: GSE39733, which can be accessed at http://www.ncbi.nlm.nih.gov/geo/query/acc.cgi?acc=GSE39733.

Sequence Analysis—The secondary structure of FAM60A sequences was predicted with HHPred server (35).

Real-time PCR and Primer Sequences—RNA was purified using TRIzol (Invitrogen), followed by subsequent DNase I digestion and clean up through an RNeasy clean up column (Qiagen). Alternatively, RNA was collected using TRIzol and then purified using the Direct-zol kit (Zymo Research). cDNAs were made using the GeneAmp kit (Applied Biosystems) using random hexamers. Real-time PCR was performed using a BioRad iCycler machine and SYBR green. Cycling conditions are as follows: 3 min at 95 °C, then 41 cycles of: 10 s at 95 °C, 30 s at annealing temperature, and 30 s at 72 °C, then followed by a melt curve. Sequences of primers and annealing temperatures are as follows: FAM60A (Origene): forward 5′-GACTCGTTCAGGAGACATCTGC-3′, reverse 5′-AGTCTTTAGACTGGGTCCAGCC-3′ (annealing at 58 °C); GAPDH: forward 5′-TCCTGCACCACCAACTGCTTAG-3′, reverse 5′-GTAGAGGCAGGGATGATGTTC-3′ (annealing at 58 °C or 60 °C); TGFβR1 (Origene): forward 5′-GACAACGTCAGGTTCTGGCTCA-3′, reverse 5′-CCGCCACTTTCCTCTCCAAACT-3′ (annealing at 60 °C); TGFβ1: forward 5′-TACCTGAACCCGTGTTGCTCTC-3′, reverse 5′-GTTGCTGAGGTATCGCCAGGAA-3′ (annealing at 60 °C); TGFβ2: forward 5′-AAGAAGCGTGCTTTGGATGCGG-3′, reverse 5′-ATGCTCCAGCACAGAAGTTGGC-3′ (annealing at 60 °C); SMAD2 (Origene): forward 5′-GGGTTTTGAAGCCGTCTATCAGC-3′, reverse 5′-CCAACCACTGTAGAGGTCCATTC-3′: ING2: forward 5′-ACATGCAGAGGAACGTGTCTGTG-3′, reverse 5′-ACCAATTCGAGCATTTGTGTAAC-3′.

Chromatin Immunoprecipitation (ChIP)—ChIP was performed as described previously (15). Precipitated DNAs were quantified by real-time PCR. PCR cycling conditions were identical to those used for real-time PCR. Primers used: SMAD2-prom-F: 5′-CCGTAGGCAAAGGGAGGTGGGGA-3′, SMAD2-prom-R: 5′-TTAGGGCGCGAGGCACGCCGGCCGA-3′ (annealing 65 °C); TGFβR1-promoter-F: 5′-CAGCCAATGGACGCGCTCCT-3′, TGFβR1-promoter-R: 5′-CACCCCAGCAAACCTCGCCT-3′ (annealing at 60 °C). TGFβ1 promoter-F: 5′-TGTTTCCCAGCCTGACTCTCCTT-3′, TGFβ1-promoter-R: 5′-ACCAAAGCGGGTGATCCAGAT-3′.

RESULTS

Proteomics Analysis of Sin3 Complexes Reveals a New Interacting Protein Named Family with Sequence Similarity 60, Member A—To expand the network of the Sin3/HDAC complex, we selected and purified six of the known core subunits (BRMS1, BRMS1L, ING2, SAP30, SAP30L and HDAC1) of the Sin3/HDAC complex. We performed at least three replicates for each of the baits to ensure good reproducibility of the data. To control for nonspecific proteins, we additionally performed ten purifications from a control 293T cell line. A total of 29

purifications (including replicates) were carried out, which led to a total of 3345 identified proteins (Supplemental Tables S1 and S2).

Quantitation was performed using label-free spectral counting. The number of spectra identified for each protein was used to calculate the normalized abundance factors. *NSAF7* software developed in house (36, 37) was used to create the Supplemental Tables S1 and S2, which report the peptides identified in each of the proteins and distributed normalized spectral abundance factor (dNSAF) values.

Next, we extracted the contaminants as described in Mosley *et al.* (38). The nonspecific proteins were extracted from the data by comparing the dNSAF value in each of the individual purifications with the dNSAF values from the controls. A protein was considered specific to a particular purification if the dNSAF value in the purification was at least two times higher than the dNSAF value in the controls. Nonspecific proteins were replaced with 0 for the subsequent analysis. After extracting the contaminants, a total of 2391 proteins remained for the further analysis (Supplemental Table S2, worksheet 2). In order to reduce the data to the most information rich group of proteins we concentrated only on the proteins that were detected in at least half of the replicates. The resulting 27 proteins remaining after the cut-off included all previously reported subunits of the Sin3/HDAC complex (Fig. 1*A*) and other additional proteins (FAM60A, TNRC18, BAHCC1, IPO8, IRS4, MRPS26, and PRPF4B) that were not previously characterized as subunits of the Sin3/HDAC complex.

Among these newly identified proteins, FAM60A (GenBank identifier 10864049) was the most abundant protein in the group and consistently copurified with known Sin3 components from 293 cells but did not purify with HDAC3 which is not a component of Sin3 complexes (Fig. 1*A*, Supplemental Fig. S1, Supplemental Tables S1 and S2 and data not shown). The relative abundance of FAM60A in relationship with the subunits of Sin3/HDAC complex is represented in Supplemental Fig. S1 with corresponding standard deviation values. Human and mouse FAM60A are proteins of about 25 kDa and have other names (C12ORF14, TERA, L4). A SAP25 subunit (GenBank identification #123778626) of the same molecular weight has been reported in some Sin3 complexes (39). However, we have not detected peptides for SAP25 in our Sin3/HDAC complex purifications from 293T cells. In the remainder of this study, we focused on the function of FAM60A using AP-MS combined with systematic functional analyses.

FAM60A Sequence Conservation—To gain more information on FAM60A, we looked at its protein sequence. FAM60A has been defined computationally by similarity of homologs in several mammals. Functional information on FAM60A is lacking, although the RNA encoding FAM60A protein was enriched in lung cancer cell lines as well as some primary cancers (Petroziello *et al.*, 2004). Sequence similarity search indicated that FAM60A homologs are found in all vertebrate and most invertebrate genomes that have been completely sequenced. In almost all cases, there is a single representative member of this family in the genome, except for frog *X. tropicalis* and zebrafish *D. rerio,* which have two. Primitive chordates (lancelet, acorn worm and sea urchin) also have a FAM60A homolog, as do arthropods, sea anemone, and most likely flatworms (a partial sequence from *Schistosoma*) (Supplemental Fig. S2). On the other hand, no FAM60A homologs were detected in *C. elegans* and other nematodes.

Analysis of sequence conservation in all of these members of the FAM60A family reveals that the protein includes three regions: the N-terminal and C-terminal highly conserved segments that exhibit high sequence conservation in all metazoans, and the middle region that is conserved across vertebrates but is replaced by a nonconserved spacer of variable length in invertebrates (Supplemental Fig. S2). Each of the two conserved terminal segments has several invariant cysteine residues, and parts of both regions are predicted to contain several beta-strands, suggesting that the ends of the protein chain might form a mixed beta-sheet together. The N-terminal region also contains several predicted alpha-helices. The loops between these elements are also very well conserved. Overall, there is 60% identity in the regions between human and sea anemone proteins, 100% identity between human, rat, mouse, and cow and 100% identity between one of the two frog and zebrafish proteins (Supplemental Fig. S2). In contrast, the central region of the FAM60A proteins is not predicted to adopt a pronounced secondary structure, even in the mammalian homologs, suggesting that its structure is stabilized by interaction with other Sin3 components.

However, we did not identify any known protein domains in FAM60A, nor does FAM60A have significant homology to other proteins in the human proteome. Thus because of the unique sequence of the protein, we chose to look at its biological function to better understand its potential role in cancer. First, we raised antisera to FAM60A and verified that it specifically recognized recombinant and native forms of FAM60A (Supplemental Fig. S3*A*, S3*B*). Next, we used this antibody to analyze FAM60A protein expression across cancer cell lines (Fig. 1*B*). We found FAM60A protein levels to be variable across cell lines, with the highest levels present in human embryonic kidney (293-FRT), lung cancer (A549), and pancreatic cancer (Capan-2) cell lines.

FAM60A is a Component of Active Sin3 Complexes—Our studies revealed that endogenous FAM60A consistently purified with various members of the Sin3 complex. To test if FAM60A would reciprocally purify Sin3 complexes, we biochemically purified through FAM60A using 293T cells that stably express a FLAG-tagged version (Supplemental Fig. S3*A*). We found that FLAG tagged FAM60A associates predominantly with components of the Sin3/HDAC complex in purifications from either nuclear or whole cell extracts (Figs. 1*C*, 1*D* and Supplemental Table S3). For visualization purposes we represented in Fig. 1*D* only the proteins that were

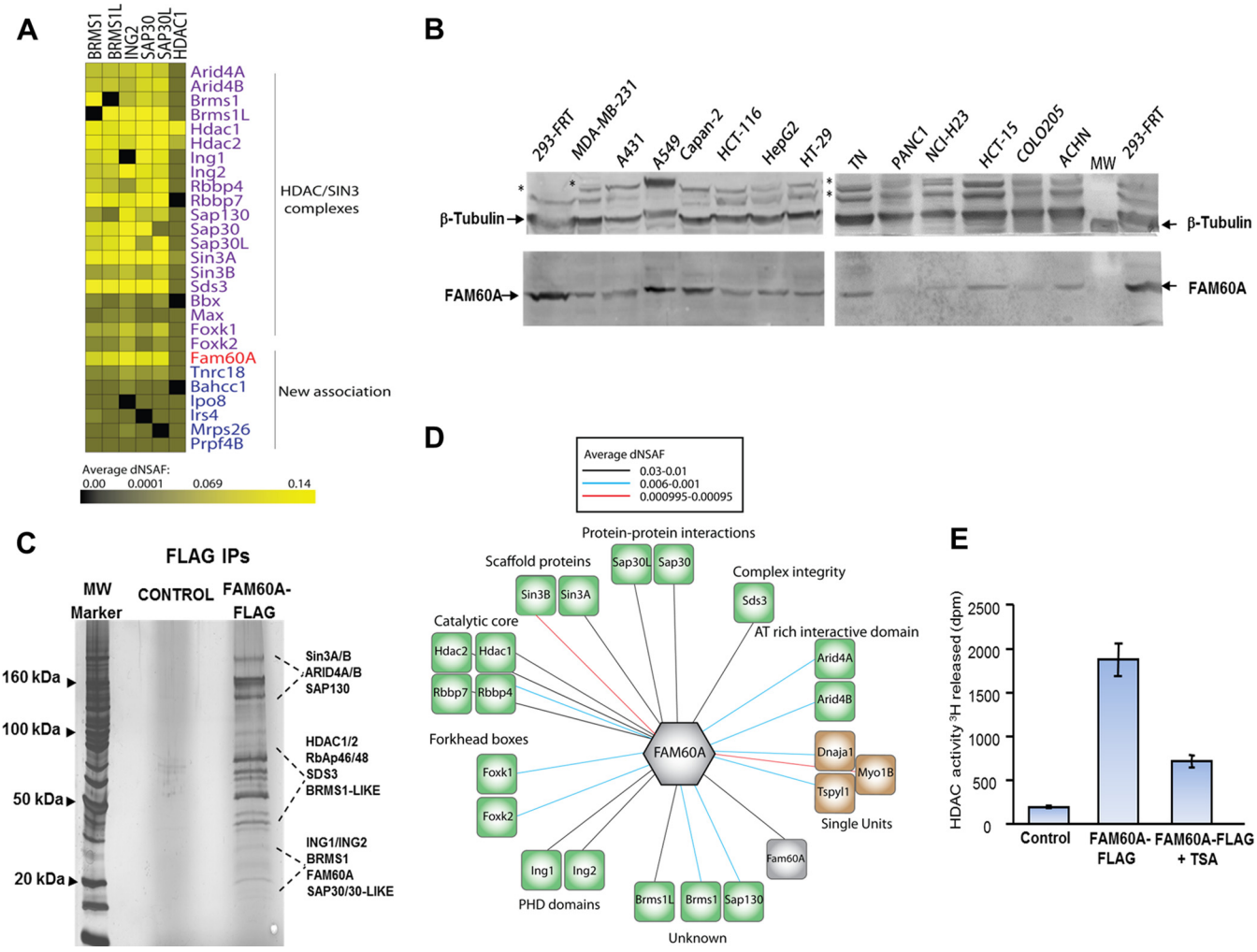

FIG. 1. **FAM60A is a metazoan-specific Sin3/HDAC interacting protein.** *A*, Heat map for the relative protein abundances expressed as dNSAF in the core Sin3/HDAC complex. The data are represented in a bait-prey matrix, where each column corresponds to purification of a bait protein and each row corresponds to a prey protein: values are average dNSAF for each protein. Color intensity represents protein abundance with brightest yellow indicating highest abundance and decreasing intensity indicating decreased abundance. Black indicates that the protein was not detected in the particular purification. Prey proteins were separated into two groups based on prior knowledge (*i.e.* known interactions colored in purple and new interactions colored in blue). *B*, Western blots showing FAM60A protein levels across several human cancer cell lines. MW = molecular weight marker. Beta-tubulin is used as a loading control; asterisks (*) denote potential modified forms of beta-tubulin. *C*, Silver stain analysis of FAM60A-FL complexes purified from 293T cells. *D*, Interaction network of the FAM60A protein and its associated proteins identified by MudPIT. The highest abundance proteins (top 22 sorted proteins) identified in two replicates of the FAM60A bait are illustrated in the figure. The bait protein is depicted as a hexagon, preys are denoted by squares. The color green denotes subunits of the Sin3/HDAC complex and the color brown indicates new associations with the FAM60A bait. Edges are colored based on the average dNSAF values. Black lines correspond to interactions with the highest abundance and red lines represent interactions with decreased abundance as shown in top left of (*A*). Identified proteins were grouped according to the functional classification. *E*, HDAC activity on ^{3}H acetylated core histones with FAM60A-FL purified complexes or control purifications. 1 μM TSA was added to the deacetylation reaction where indicated.

detected in two replicates and that were the most highly enriched (based on dNSAF average values) in the FAM60A purifications. The remaining proteins identified in two replicates using FAM60A as the bait are reported in the Supplemental Table S3. FAM60A complexes show nearly identical banding patterns to purifications of Sin3 subunits ING2 and BRMS1, which we previously purified (Fig. 1*C*) (15). Therefore, FAM60A is a component of Sin3/HDAC complexes in humans and our data suggest that it does not form other major complexes in 293T cells.

To test if FAM60A associates with deacetylase activity, we performed HDAC assays on core histones using FAM60A-FLAG complex purified from 293T cells. Indeed, the purified FAM60A contains deacetylase activity which is sensitive to trichostatin A (TSA), an HDAC inhibitor (Fig. 1*E*). FLAG purifications using a control 293 cell line lacking tagged FAM60A

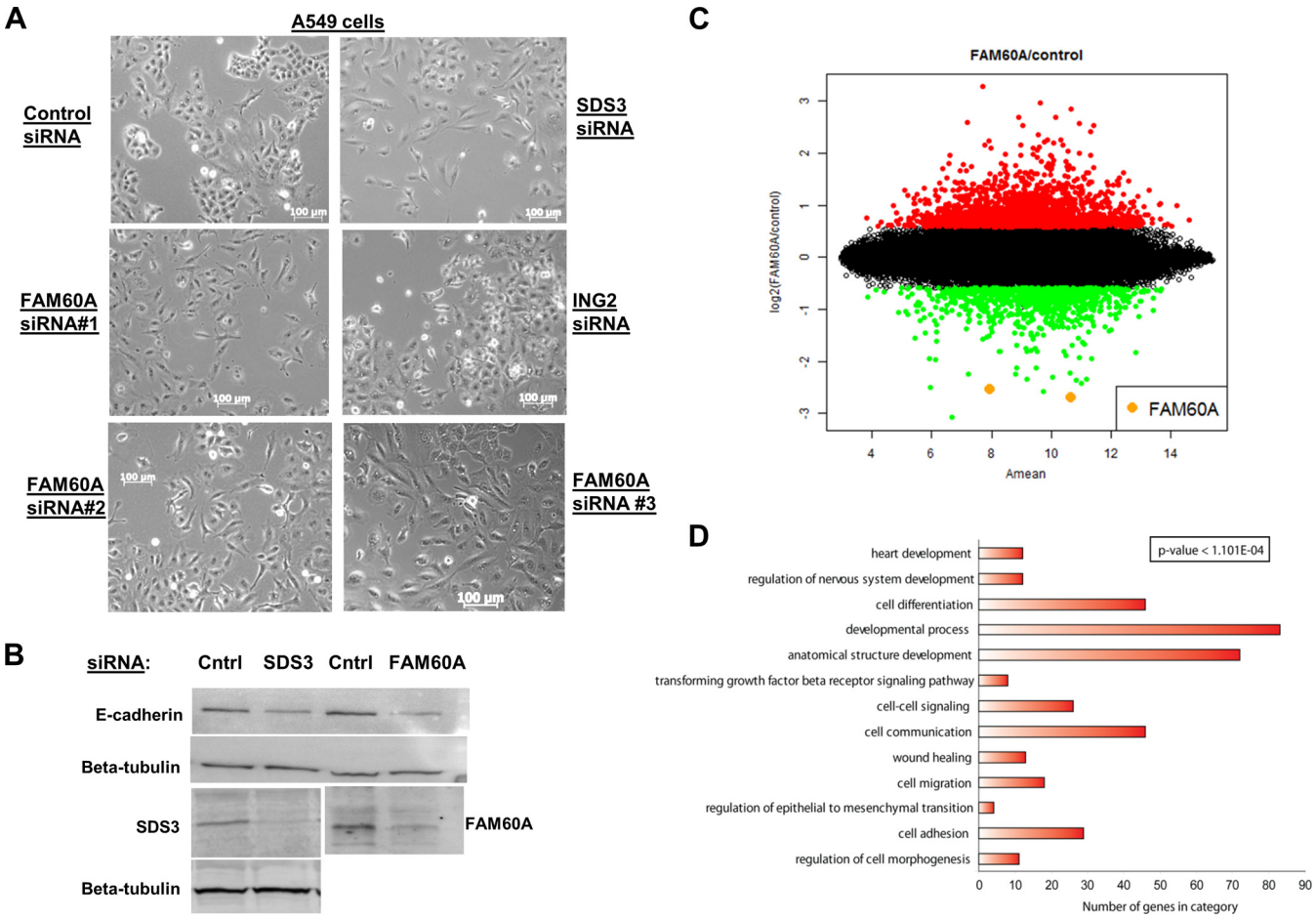

FIG. 2. **Loss of FAM60A affects cell morphology and gene expression.** *A*, A549 cells were transfected with control siRNAs, or siRNAs against FAM60A, SDS3, or ING2. *B*, Western blots of whole cell extracts from FAM60A, SDS3, and control knockdown using the indicated antibodies. *C*, The gene expression response of FAM60A knockdown relative to a nontargeting control is shown in the plot. The *y*-axis indicates the ratio of expression as log2(FAM60A knockdown/control), whereas the combined signal from both samples is plotted on the *x*-axis as 0.5 *(log2(FAM60A knockdown)+log2(control)). The top differentially expressed genes were selected by requiring an expression difference of at least 1.5-fold and applying an adjusted *p* value cut-off of 0.05. Probes corresponding to FAM60A are highlighted on the plot. *D*, A subset of go terms identified in microarray analysis in FAM60A knockdown cells.

did not contain HDAC activity (Fig. 1*E*). Thus FAM60A is a novel component of catalytically active Sin3 complexes.

FAM60A Affects Cancer Cell Morphology—To better understand the function of FAM60A, we chose to knock it down using siRNAs in A549 lung cancer cells. Interestingly, we found that cells transfected with three different siRNAs against FAM60A showed an altered cell morphology to varying degrees in the population (Figs. 2*A*, 2*B*, Supplemental Fig. S4*A*, S4*B*). FAM60A knockdown cells appeared elongated and more spread out on the plate than control cells. To see whether the FAM60A knockdown phenotype is because of its role in the Sin3 complex, we also knocked down SDS3, a core subunit that is required for the integrity and activity of the complexes (9, 10). Indeed, the morphology change in SDS3 knockdowns was similar to what we observed in FAM60A knockdown cells, suggesting that loss of FAM60A is causing these morphological effects by disrupting its role in the Sin3 complex (Fig. 2*A*, 2*B*). We also observed a decrease in E-cadherin protein levels in FAM60A and SDS3 knockdown cells, which is a protein important for maintaining cell to cell contacts (Fig. 2*B*) (40).

Knockdown of ING2, however, did not affect morphology of the A549 lung cancer cells (Fig. 2*A*, Supplemental Fig. S4*C*). This suggested that different subunits in the Sin3 complex are only required for some functions of the complex. This is in agreement with studies showing that loss of ING2 does not disrupt the rest of the Sin3 complex and that ING2's main role is to target the complex to a specific subset of genes (15, 41). Therefore, the alteration in cell morphology is because of a function of the complex that requires FAM60A and the Sin3/HDAC core machinery, but not ING2.

FAM60A Represses Gene Expression and Regulates a Specific Subset of Genes—To better understand the molecular changes occurring in these cells, we used microarrays to compare gene expression patterns between control knockdown A549 cells and FAM60A knockdown cells (Figs. 2*C*, 2*D*,

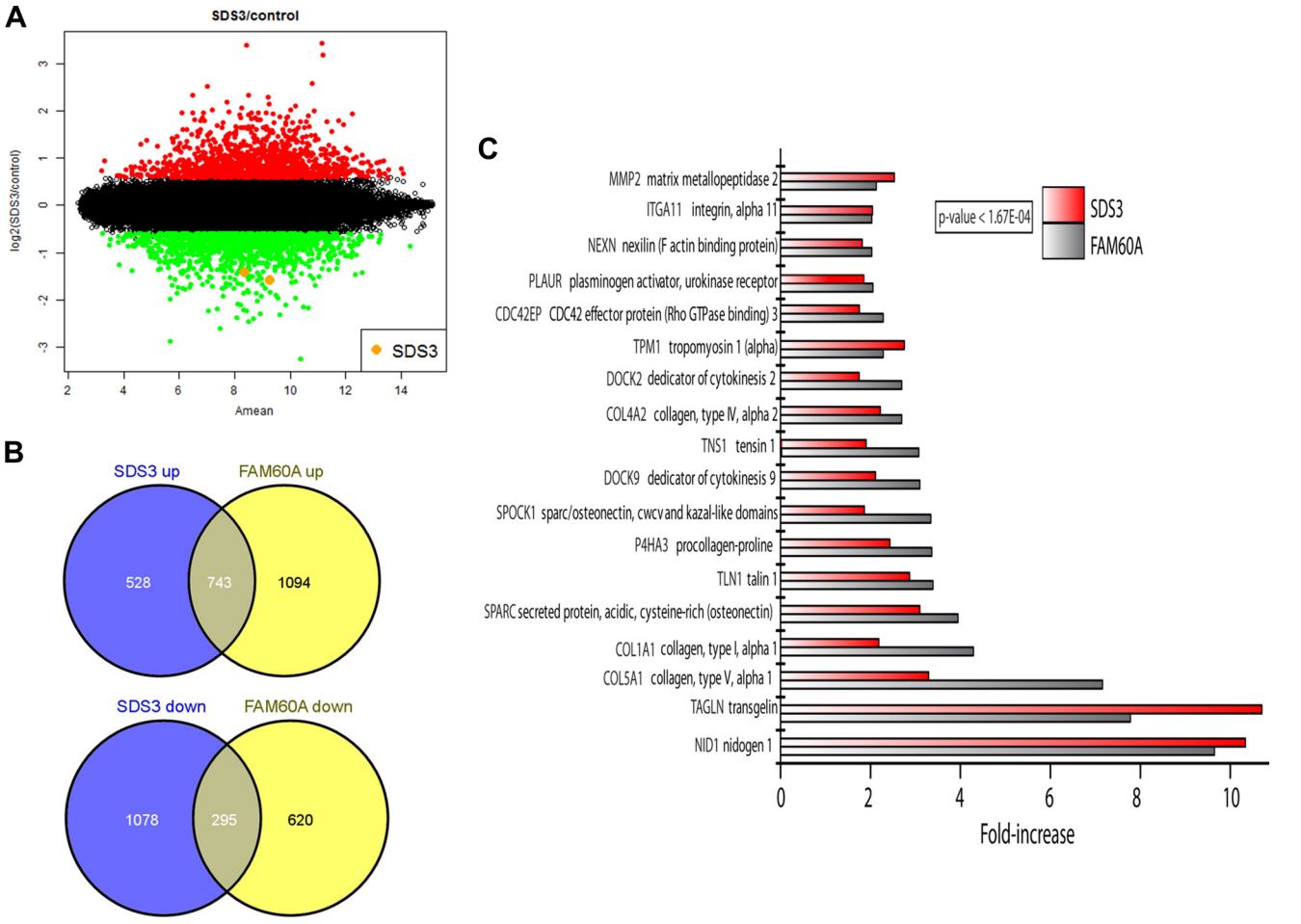

FIG. 3. **FAM60A and SDS3 regulate common subsets of genes.** *A*, Scatter plot showing the changes in gene expression in SDS3 knockdown cells relative to a nontargeting control siRNA. The *y*-axis indicates the ratio of expression as log2 (SDS3 knockdown/control), whereas the combined signal from both samples is plotted on the *x*-axis as 0.5 *(log2(SDS3 knockdown) + log2(control)). The top differentially expressed genes were selected by requiring an expression difference of at least 1.5-fold and applying an adjusted *p* value cut-off of 0.05. Probes corresponding to SDS3 are highlighted on the plot. *B*, The number of genes enriched in common on knockdown of either FAM60A or SDS3 is shown in the Venn diagram. The top gene set for each knockdown was identified using the criteria described in (*A*). The significance of the degree of overlap was assessed using the hypergeometric distribution and returned a *p* value of $< 2.22e\text{-}16$. *C*, Bar graph showing the genes that were up-regulated in both FAM60A and SDS3 knockdown cells with functions related to cell migration or extracellular matrix (ECM) structure. The fold-increase of the top probe for each gene is shown. A 1.5-fold cutoff was used and all genes shown have a *p* value of less than 1.67e-04.

GEO accession # GSE39733 which can be accessed at http://www.ncbi.nlm.nih.gov/geo/query/acc.cgi?acc=GSE39733). Gene expression analysis revealed that FAM60A RNA levels were decreased ~sixfold 3 days after transfection (Fig. 2*C*). The majority of genes that changed in expression were increased in FAM60A knockdowns (Fig. 2*C*). This was not surprising because the Sin3/HDAC complex is known to play a repressive role in transcription. We focused on genes that were increased in expression in FAM60A knockdown cells because this group likely contained direct targets of the FAM60A/Sin3 complex. In FAM60A knockdown cells, 1837 probes increased in expression more than 1.5-fold (Fig. 2*C*). Indeed, consistent with the observed change in cell morphology, many of these genes were related to cell morphogenesis, cell adhesion, regulation of epithelial to mesenchymal transition (EMT), cell migration and wound healing (Fig. 2*D*). Additionally, many genes that increased in FAM60A knockdown cells were involved in regulating cell signaling (especially the TGF-beta pathway) and developmental processes (Fig. 2*D*).

We then tested SDS3 knockdown cells for comparison with FAM60A regulated genes and found that approximately half of the genes that were changed more than 1.5-fold were up-regulated (1271 up, 1373 down) (Fig. 3*A*). We then compared these two data sets and found that a significant portion of genes that changed (either up or down) was conserved between data sets (Fig. 3*B*). This was expected as both proteins are members of the Sin3 complex and the data further supports the notion that the cellular effects of depleting FAM60A are because of its role in the Sin3 complex.

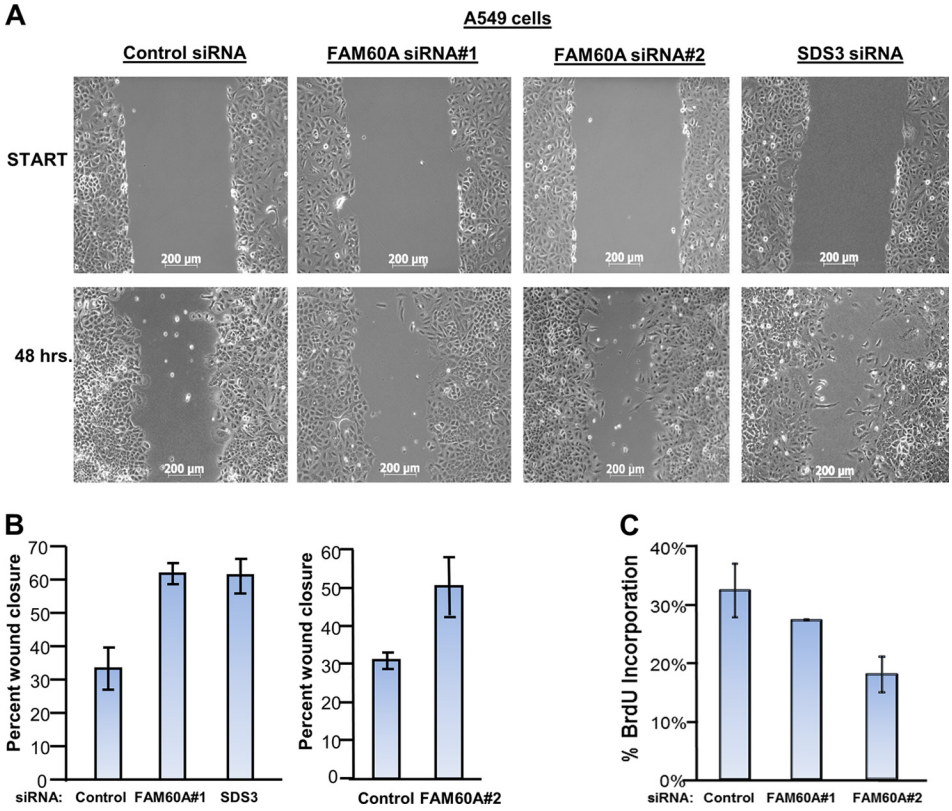

FIG. 4. **Loss of FAM60A or SDS3 increases cell migration in A549 lung cancer cells.** *A*, Migration assays in control, FAM60A, or SDS3 knockdown cells. A representative example is shown for each siRNA. *B*, Quantification of migration assays shown in (*A*). The average of at least triplicate biological replicates is shown. Error bars represent plus/minus one average deviation. *C*, Percent BrdU incorporation in A549 cells transfected with control siRNAs or siRNAs against FAM60A. Bars represent the average BrdU incorporation of three biological replicates, error bars represent ± one standard deviation.

Interestingly, we found that many of the highest differentially expressed probes (by fold-change) in both FAM60A and SDS3 knockdown cells are known positive markers of mesenchymal cells or have functions related to cell migration or extracellular matrix composition (Fig. 3*C*) (42, 43). This includes three genes that were among the top changed genes in both the FAM60A and SDS3 microarrays: Nidogen/entactin, transgelin, and collagen type V alpha 1 (Fig. 3*C*). Nidogen/entactin is normally synthesized by mesenchymal cells and helps to bridge components of the extracellular matrix (44). Transgelin promotes cancer stem cell migration and invasion (45). Collagens are also involved in cell migration and forming extracellular matrix structures (42). Expression levels of several collagens were increased in FAM60A and SDS3 knockdowns, including Collagen, type V, alpha 1 (Fig. 3*C*).

Because many genes induced by loss of FAM60A and SDS3 were involved in cell migration, we wanted to know if FAM60A and SDS3 knockdown cells had increased motility. To answer this question, we used a scratch assay/wound healing assay. We quantified percent scratch closure by measuring the open area of the scratch at time zero and 1 and 2 days post scratching. A549 cells are known to be somewhat motile (46), and we observed a 35% wound closure 2 days after scratching in control knockdown cells (Figs. 4*A*, 4*B*). However, we observed a 50–60% wound closure by 2 days post scratch in FAM60A knockdown cells using two different siRNAs against FAM60A (Figs. 4*A*, 4*B*). We verified that wound closure was because of increased migration of the cells, as we did not observe an increase in proliferation in FAM60A knockdown cells (Fig. 4*C*). We then tested the role of SDS3 in cell migration and found a similar increase in cell migration in SDS3 knockdown cells (Figs. 4*A*, 4*B*). Therefore, loss of FAM60A or disruption of the core of the Sin3 complex leads to an increase in the migration of lung cancer cells.

Next, we asked if FAM60A could affect cell morphology and migration in a distinct cell type. We chose to use HepG2 liver cancer cells, which have a moderate level of FAM60A protein expression (Fig. 1*B*). Indeed, we saw that loss of FAM60A induced a change in cell morphology and a decrease in E-cadherin (Figs. 5*A*, 5*B*). We also found that loss of FAM60A increased migration of HepG2 cells (Figs. 5*C*, 5*D*, Supplemental Fig. S5*A*). BrdU staining of FAM60A knockdown HepG2 cells confirmed that wound closure was indeed because of increased migration and not proliferation (Fig. 5*E*, Supplemental Fig. 5*B*). These data demonstrate that FAM60A can affect cell morphology and migration in distinct cell types.

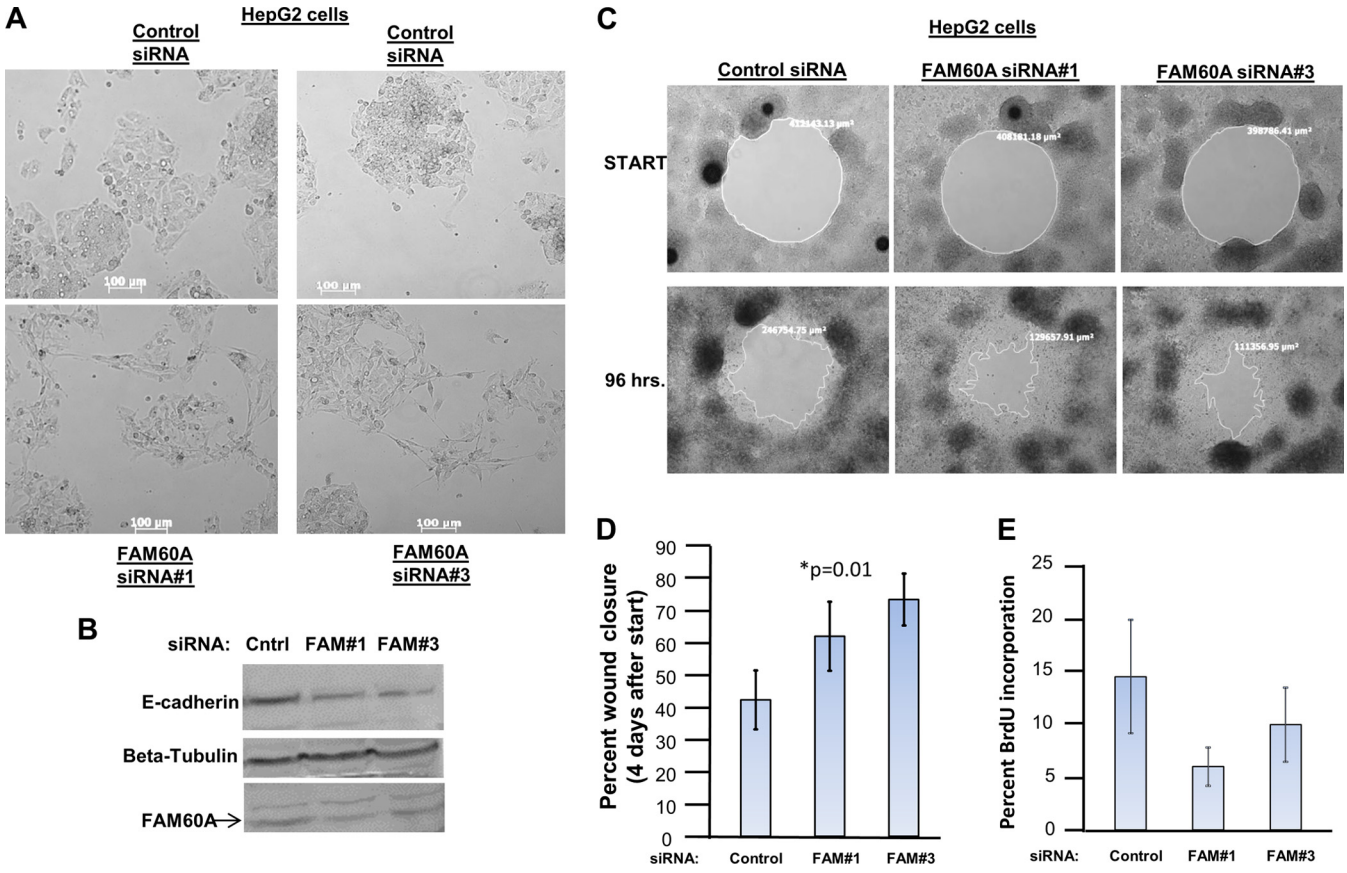

FIG. 5. **FAM60A regulates cell morphology and migration of HepG2 cells.** *A*, Morphology changes in HepG2 cells transfected with control siRNAs or siRNAs against FAM60A. *B,* Western blots of whole cell extracts from HepG2 knockdown cells using the indicated antibodies. *C*, Migration assays in HepG2 knockdown cells transfected with control siRNAs or siRNAs against FAM60A. A representative example is shown. *D*, Quantification of HepG2 migration assays. The average from several independent transfections is shown (control siRNA $n = 5$; FAM60A siRNA#1 $n = 7$; FAM60A siRNA#2 $n = 4$); error bars represent ± one standard deviation. The p value was calculated using a two-tailed t test. *E*, BrdU incorporation was measured in HepG2 cells transfected with control siRNAs or siRNAs against FAM60A. Bars represent the average of six independent transfections for each siRNA ± one standard deviation.

FAM60A Directly Regulates the Expression of Genes Encoding Components of the TGF-beta Signaling Pathway—Our microarray experiments in A549 FAM60A and SDS3 knockdown cells revealed that many of the genes altered in expression were involved in cell migration. Thus, we looked in more detail at the signaling pathways altered in the FAM60A and SDS3 knockdown gene expression microarrays. Interestingly, probes for several genes encoding components of the TGF-beta signaling pathway were increased in both SDS3 and FAM60A knockdown cells, including TGF-beta receptor 1 (TGFβR1), SMAD2, and the gene encoding the ligand TGF-beta1 (Fig. 6*A*). We confirmed the up-regulation of some of these genes by real-time PCR and verified their up-regulation using independent siRNA sequences against FAM60A (Supplemental Fig. S5*C*–S5*E*). We then tested if FAM60A regulates TGF-beta pathway genes in HepG2 cells. Indeed, we found that loss of FAM60A induced the genes encoding TGFbeta 1 and TGFbeta 2 in HepG2 liver cancer cells (Supplemental Fig. S5*F*–S5*H*) consistent with their morphology change and increased migration.

Interestingly, TGF-beta is known to induce cell migration in A549 cells and other cell types (47). Additionally, expression of the top three genes that were increased in the FAM60A microarray (nidogen/entactin, transgelin and collagen V) have been shown to increase on stimulating the TGF-beta pathway and are also up-regulated on SDS3 knockdown (Fig. 3*C*) (43, 46). Because these genes are known downstream targets of TGF-beta, our microarrays suggested that increases in TGF-beta pathway components may be one of the earlier events occurring when FAM60A levels are reduced. The data also support a model where small changes in TGF-beta pathway genes can have large downstream effects. This is consistent with data showing that exogenous TGF-beta1 can induce expression of genes in the TGF-beta pathway in this cell line (43), suggesting a positive feedback mechanism through this pathway.

Because several genes encoding components of the TGF-beta pathway were increased in expression level, we next asked if they were direct targets of FAM60A. We performed ChIP assays with FAM60A antisera and observed binding at

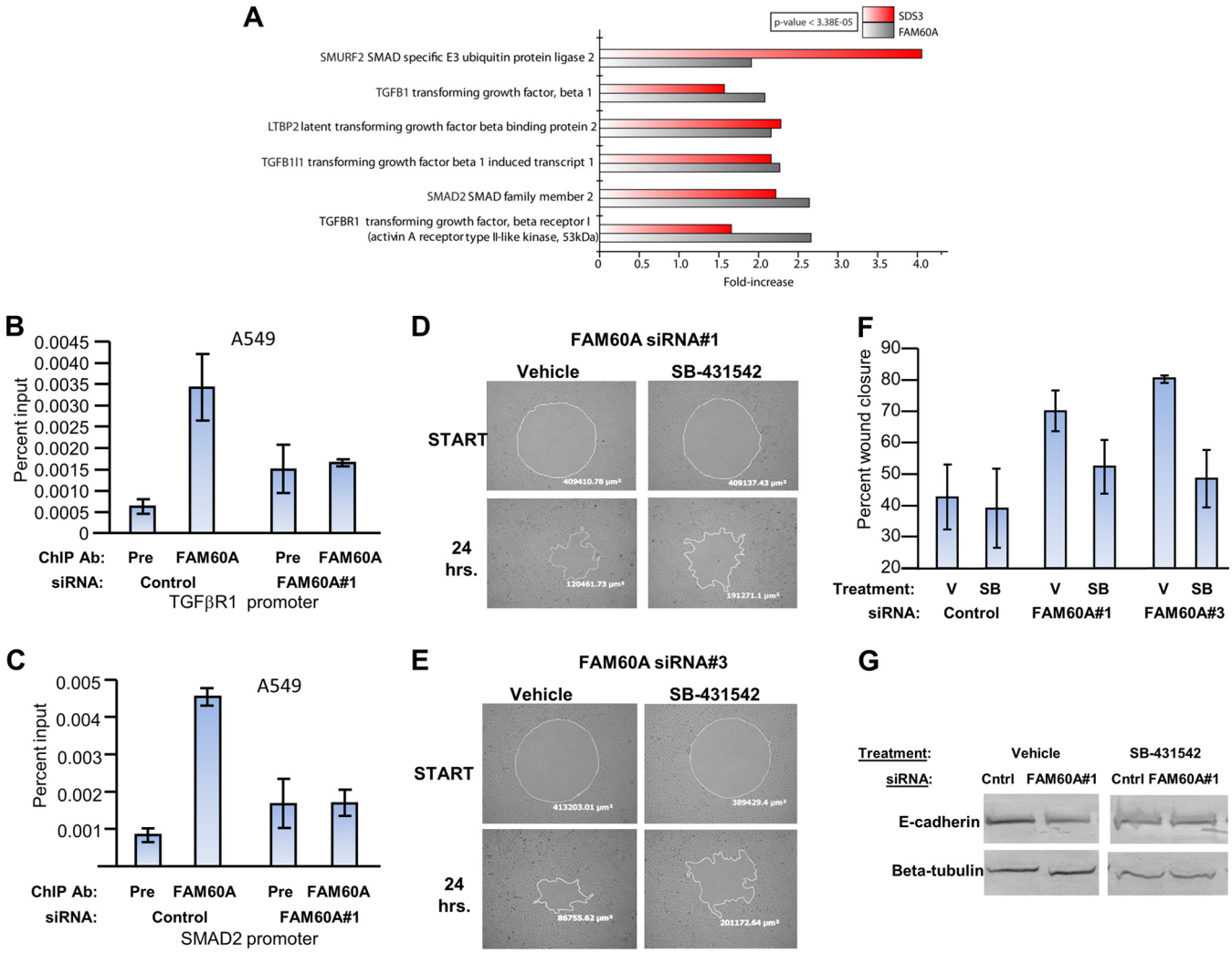

FIG. 6. **FAM60A directly represses expression of genes in the TGF-beta pathway.** *A*, Genes increased by microarray analysis in FAM60A and SDS3 knockdown cells that encode components of the TGF-beta signaling pathway. Fold-increase of the top probe for that gene is shown. A 1.5-fold cutoff was used and all genes shown have a *p* value of less than 3.38e-05. *B*, *C*, Chromatin immunoprecipitation (ChIP) assays in control or FAM60A knockdown cells at the TGF-beta receptor 1 promoter (*B*) or SMAD2 promoter (*C*). Error bars represent ± one standard deviation of triplicate real-time PCR reactions. *D*, *E*, Migration assays in FAM60A knockdown cells in the presence of vehicle or SB-43152. A representative example for each siRNA against FAM60A is shown. *F*, Quantification of migration assays in FAM60A knockdown cells in the presence of vehicle (V) or SB-431542 (SB). Bars represent the average of at least three monitored scratches. Error bars represent plus/minus one average deviation. *G*, Western blots using the indicated antibodies in vehicle treated FAM60A knockdown cells and SB-431542 treated knockdown cells.

both the TGFβR1 and SMAD2 promoters, two genes that were increased in FAM60A knock-down cells (Figs. 6*B*, 6*C*). FAM60A binding was diminished at these promoters in FAM60A knockdown cells, showing the specificity of the antisera (Figs. 6*B*, 6*C*). Therefore, FAM60A is normally bound to TGFβR1 and SMAD2 promoters in A549 lung cancer cells and is important for their transcriptional repression.

The Sin3 complex contains at least 15 subunits, thus we were interested to determine if ING2 was regulating TGF-beta related genes, because ING2 knockdown cells did not show a change in cell morphology. We found that knockdown of ING2 was insufficient to up-regulate SMAD2, TGFβ1, or TGFβR1 transcript levels (Supplemental Fig. S6*A*). Since ING2 is known to play a role in recruiting the Sin3 complex to specific genes, we looked at its occupancy at these genes. ING2 binding was only detected at one out of the three FAM60A and SDS3-regulated genes tested (Supplemental Fig. S6*B*). Thus, different subunits of the complex can affect expression of specific subsets of genes.

Next we looked at FAM60A's role in the Sin3 complex in more detail. Because it was clear that FAM60A was important for regulating TGF-beta related genes, we asked if it was responsible for the recruitment of Sin3 complexes to chromatin. However knockdown of FAM60A did not alter the binding of Sin3a or SAP30 to the TGFβR1 promoter (Supplemental Fig. S7*A*). In agreement with this, we found that FAM60A does

not play a major structural role in the Sin3 complex. Complexes purified from FAM60A knockdown cells still contain HDAC1 and Sin3a and show nearly identical silver stain banding patterns to control complexes (Supplemental Fig. S7*B*, S7*C*). Thus FAM60A likely plays a special role in modulating transcriptional activity through a yet unknown mechanism.

Induction of Cell Migration in FAM60A Knockdowns is Because of Increased TGF-beta Signaling—Loss of FAM60A leads to an increase in cell migration in A549 lung cancer cells and HepG2 liver cancer cells and increases expression of TGF-beta pathway genes. Interestingly, treating A549 cells with exogenous TGF-beta can induce cellular changes such as epithelial to mesenchymal transition and increase the migratory ability of A549 cells (48, 49). Therefore, we asked if the phenotypic changes seen in FAM60A knockdowns were because of increased TGF-beta signaling. To test this, we used a well-characterized TGF-beta receptor I inhibitor, SB-431542 (48, 50). This molecule blocks the kinase activity of the receptor and is effective in blocking downstream SMAD signaling as well as EMT, migration and invasion induced by TGF-beta (48, 50). We first verified in our hands that SB-431542 can prevent TGF-beta induced morphology changes in TGF-beta treated A549s. In agreement with published observations (48, 50), cells treated with TGF-beta underwent an elongation and morphology change, whereas those treated simultaneously with TGF-beta and 2 μM SB-431542 maintained normal morphology (Supplemental Fig. S8*A*).

To test if SB-431542 could prevent the morphology change because of knockdown of FAM60A, we added the inhibitor (or vehicle) 1 day after siRNA transfection and monitored cell morphology. Indeed, in FAM60A knockdown cells treated with SB-431542, we observed a suppression of the phenotypic change seen after FAM60A knockdown (Supplemental Fig. S8*B*, S8*C*, S8*D*). Therefore, intact TGFbeta receptors and downstream TGF-beta signaling are required for the change in cell morphology seen on loss of FAM60A.

Next, we asked if the TGF-beta inhibitor could suppress migration induced by loss of FAM60A (Figs. 6*D*, 6*E*, 6*F*). We treated A549 cells with SB-431542 or vehicle at 1 day after transfection and induced wounds 2 days after transfection. We monitored wounds for an additional day after. Indeed, addition of the TGF-beta receptor inhibitor suppressed the migration in FAM60A knockdown cells (Figs. 6*D*, 6*E*, 6*F*, Supplemental Figs. S8*E*, S8*F*). SB-431542 was also effective in maintaining normal E-cadherin levels in FAM60A knockdown cells (Fig. 6*G*). These results suggested that increased TGF-beta signaling mediates the migration and induced morphological changes seen in FAM60A knockdowns and that intact TGF-beta receptors are required for downstream morphological changes to occur in FAM60A knockdowns.

FAM60A's role in repressing transcription of TGFbeta pathway genes was particularly interesting, because some cancer cells have inactivated or mutated TGF-beta receptors (51). We reasoned that if FAM60A was directly modulating expression of components of the TGF-beta pathway, then FAM60A should affect their transcription in multiple cell types, regardless of their TGF-beta receptor status. To test this, we used HCT116 colon carcinoma cells which have a mutated TGF-beta receptor 2 and are not responsive to exogenous TGF-beta (52). Indeed, we found that the genes encoding the TGFβ1 and 2 ligands were both transcriptionally induced by knockdown of FAM60A in this cell line (Supplemental Fig. S9*A*–S9*C*). However, no EMT-like change in cell morphology was observed (Supplemental Fig. S9*D*). Thus, FAM60A can directly regulate genes in the TGF-beta pathway in multiple cell types, despite the overall TGF-beta responsiveness of the cell type to TGF-beta stimuli. However, the change in cell morphology and other downstream events are dependent on functional TGFbeta 1 and 2 receptors. Together, these results reveal that FAM60A and the core Sin3 machinery are required to repress transcription of genes encoding components of the TGF-beta signaling pathway and in turn, suppress cell migration.

DISCUSSION

As proteomics studies reveal the existence of many proteins with unique sequences, the functional characterization of these proteins becomes increasingly important. Here, our studies revealed that an uncharacterized protein FAM60A, is a subunit of the Sin3 deacetylase complex and is important for the repression of genes encoding components of the TGF-beta signaling pathway. FAM60A is a metazoan-specific protein that is uniquely found in the Sin3 complex and does not appear to associate with other protein complexes. While this manuscript was in revision, another group reported FAM60A as a component of Sin3 complexes and showed that FAM60A protein levels fluctuate with the cell cycle in U2OS cells (53). FAM60A was also recently found to interact with Sin3a in ES cells (54). Thus, FAM60A is a component of Sin3 complexes in multiple mammalian cell types. Its role as a metazoan specific subunit of the Sin3 complex is particularly interesting because our results implicate FAM60A in controlling TGF-beta signaling. The TGF-beta signaling pathway regulates cellular processes implicated in cancer progression and metastasis, including epithelial to mesenchymal transition and cell migration (47, 55, 56). The downstream transcriptional consequences of activating the TGF-beta pathway include deregulation of genes involved in cell migration and invasion (47, 55, 56).

Interestingly, we found that abrogating FAM60A function in A549 lung cancer cells and HepG2 liver cancer cells induced a change in cell morphology and down-regulation of E-cadherin. In addition, cancer cells depleted for FAM60A show an increased ability to migrate. These changes also occurred when SDS3, a core subunit of the Sin3 complex, was knocked down, suggesting that these functions revealed by abrogating FAM60A are attributed to its role in the Sin3 complex. Together, the data suggest that FAM60A containing Sin3 com-

plexes normally suppress cell migration, a process that can contribute to cancer cell metastasis. Interestingly the BRMS1 subunit of the Sin3 complex can suppress metastasis in mouse models (18, 57), suggesting that specific subunits in the Sin3 complex may work together to suppress metastasis.

These results were surprising because previous studies reported a reversal of EMT and inhibition of cell migration on pan-HDAC inhibitor treatment or HDAC1 knockdown (58–61). However, pan-HDAC inhibitors affect several different HDACs and HDAC1 itself has multiple functions. Our results reveal that inhibiting specific functions of the HDAC1/2 containing Sin3 complex, leads to an increase in cell migration. The change in cell morphology and induction of cell migration are only induced when specific subunits of the Sin3 complex are inhibited, as we did not observe these changes in ING2 knockdown cells. Consistent with this observation, ING2 knockdown did not increase expression of TGFβ1 or TGFβR1 transcripts. Interestingly, over-expression of ING2 can induce colon cancer cell invasion suggesting that ING2 could promote invasion and metastasis (62). These results are in accord with studies of the HDAC1/2 containing NuRD complex, which have shown that some subunits of that complex appear to be prometastatic whereas others have the opposite effect (for review see (63)). These studies suggest that inhibiting distinct HDAC1/2 complexes as well as distinct subunits in those complexes can lead to different biological outcomes. Since general HDAC inhibitors are being used as anticancer agents, it is critical to understand how the multisubunit HDAC complexes function.

Though several studies have shown that HDACi can reverse EMT, a recent study revealed that HDACi could increase metastatic potential in mice by up-regulation of a prometastatic gene Ezrin (64). It is not clear which HDACs or complexes may be mediating this effect, but our results and the work from others suggest that certain Sin3 or NuRD subunits normally work to suppress steps in the metastatic pathway (62, 65) (18). Therefore, inhibiting certain HDAC sub-complexes or subunits could increase the potential for metastasis or promote certain steps along the metastatic cascade. This is interesting in the light of recent biochemical studies, which revealed that HDAC inhibitors may preferentially target specific subunits of HDAC containing complexes (15, 17, 66). Together, these studies reveal a role for FAM60A as a transcriptional regulator and component of the human Sin3 complex and extend the known functional roles of the Sin3 complex to include suppression of cell migration.

Acknowledgments—We thank Jamie Dyer and Kenneth Lee for critical reading of the manuscript, Dr. Danny Welch (University of Kansas) for helpful discussions. We also thank the Stowers Institute microscopy center and Andrew Box in the Stowers Institute cytometry facility for training.

* This work was supported by NIGMS grant R37 GM047867 (JLW) and NCI fellowship 5F32CA130468 (KTS). KTS is the American Cancer Society's 2008 Cattle Baron's Ball of Lubbock Postdoctoral Fellow (#PF-09-109-01-GMC).

S This article contains supplemental Figs. S1 to S9 and Tables S1 to S3.

‖ Current address: Missouri State University, Springfield, Missouri 65897, USA.

** To whom correspondence should be addressed: Stowers Institute for Medical Research, Kansas City, Missouri 64110. Tel.: 816-926-4392; Fax: 816-926-4692; E-mail: jlw@stowers.org.

REFERENCES

1. Choudhary, C., Kumar, C., Gnad, F., Nielsen, M. L., Rehman, M., Walther, T. C., Olsen, J. V., and Mann, M. (2009) Lysine acetylation targets protein complexes and co-regulates major cellular functions. *Science* **325,** 834–840
2. Witt, O., Deubzer, H. E., Milde, T., and Oehme, I. (2009) HDAC family: What are the cancer relevant targets? *Cancer Letts.* **277,** 8–21
3. Yang, X. J., and Seto, E. (2008) The Rpd3/Hda1 family of lysine deacetylases: from bacteria and yeast to mice and men. *Nat. Rev. Mol. Cell Biol.* **9,** 206–218
4. Gregoretti, I. V., Lee, Y. M., and Goodson, H. V. (2004) Molecular evolution of the histone deacetylase family: functional implications of phylogenetic analysis. *J. Mol. Biol.* **338,** 17–31
5. David, G., Grandinetti, K. B., Finnerty, P. M., Simpson, N., Chu, G. C., and Depinho, R. A. (2008) Specific requirement of the chromatin modifier mSin3B in cell cycle exit and cellular differentiation. *Proc. Natl. Acad. Sci. U. S. A.* **105,** 4168–4172
6. Pile, L. A., Schlag, E. M., and Wassarman, D. A. (2002) The SIN3/RPD3 deacetylase complex is essential for G(2) phase cell cycle progression and regulation of SMRTER corepressor levels. *Mol. Cell. Biol.* **22,** 4965–4976
7. Suryadinata, R., Sadowski, M., Steel, R., and Sarcevic, B. (2011) Cyclin-dependent kinase-mediated phosphorylation of RBP1 and pRb promotes their dissociation to mediate release of the SAP30.mSin3.HDAC transcriptional repressor complex. *J. Biol. Chem.* **286,** 5108–5118
8. Lai, A., Kennedy, B. K., Barbie, D. A., Bertos, N. R., Yang, X. J., Theberge, M. C., Tsai, S. C., Seto, E., Zhang, Y., Kuzmichev, A., Lane, W. S., Reinberg, D., Harlow, E., and Branton, P. E. (2001) RBP1 recruits the mSIN3-histone deacetylase complex to the pocket of retinoblastoma tumor suppressor family proteins found in limited discrete regions of the nucleus at growth arrest. *Mol. Cell. Biol.* **21,** 2918–2932
9. Alland, L., David, G., Shen-Li, H., Potes, J., Muhle, R., Lee, H. C., Hou, H., Jr., Chen, K., and DePinho, R. A. (2002) Identification of mammalian Sds3 as an integral component of the Sin3/histone deacetylase corepressor complex. *Mol. Cell. Biol.* **22,** 2743–2750
10. Lechner, T., Carrozza, M. J., Yu, Y., Grant, P. A., Eberharter, A., Vannier, D., Brosch, G., Stillman, D. J., Shore, D., and Workman, J. L. (2000) Sds3 (suppressor of defective silencing 3) is an integral component of the yeast Sin3[middle dot]Rpd3 histone deacetylase complex and is required for histone deacetylase activity. *J. Biol. Chem.* **275,** 40961–40966
11. Ludwig, S., Klitzsch, A., and Baniahmad, A. (2011) The ING tumor suppressors in cellular senescence and chromatin. *Cell Biosci.* **1,** 25
12. Ayer, D. E., Lawrence, Q. A., and Eisenman, R. N. (1995) Mad-Max transcriptional repression is mediated by ternary complex formation with mammalian homologs of yeast repressor Sin3. *Cell* **80,** 767–776
13. Sommer, A., Hilfenhaus, S., Menkel, A., Kremmer, E., Seiser, C., Loidl, P., and Lüscher, B. (1997) Cell growth inhibition by the Mad/Max complex through recruitment of histone deacetylase activity. *Curr. Biol.* **7,** 357–365
14. Wotton, D., Knoepfler, P. S., Laherty, C. D., Eisenman, R. N., and Massagué, J. (2001) The Smad transcriptional corepressor TGIF recruits mSin3. *Cell Growth Differ.* **12,** 457–463
15. Smith, K. T., Martin-Brown, S. A., Florens, L., Washburn, M. P., and Workman, J. L. (2010) Deacetylase inhibitors dissociate the histone-targeting ING2 subunit from the Sin3 complex. *Chem. Biol.* **17,** 65–74
16. Dickinson, M., Johnstone, R. W., and Prince, H. M. (2010) Histone deacetylase inhibitors: potential targets responsible for their anti-cancer effect. *Invest. New Drugs* **28,** S3–20
17. Bantscheff, M., Hopf, C., Savitski, M. M., Dittmann, A., Grandi, P., Michon, A. M., Schlegl, J., Abraham, Y., Becher, I., Bergamini, G., Boesche, M.,

Delling, M., Dümpelfeld, B., Eberhard, D., Huthmacher, C., Mathieson, T., Poeckel, D., Reader, V., Strunk, K., Sweetman, G., Kruse, U., Neubauer, G., Ramsden, N. G., and Drewes, G. (2011) Chemoproteomics profiling of HDAC inhibitors reveals selective targeting of HDAC complexes. *Nat. Biotechnol.* **29,** 255–265

18. Seraj, M. J., Samant, R. S., Verderame, M. F., and Welch, D. R. (2000) Functional evidence for a novel human breast carcinoma metastasis suppressor, BRMS1, encoded at chromosome 11q13. *Cancer Res.* **60,** 2764–2769
19. Wu, M. Y., Eldin, K. W., and Beaudet, A. L. (2008) Identification of chromatin remodeling genes Arid4a and Arid4b as leukemia suppressor genes. *J. Natl. Cancer Inst.* **100,** 1247–1259
20. Ythier, D., Larrieu, D., Brambilla, C., Brambilla, E., and Pedeux, R. (2008) The new tumor suppressor genes ING: genomic structure and status in cancer. *Int. J. Cancer* **123,** 1483–1490
21. Unoki, M., Kumamoto, K., Takenoshita, S., and Harris, C. C. (2009) Reviewing the current classification of inhibitor of growth family proteins. *Cancer Sci.* **100,** 1173–1179
22. Unoki, M., Kumamoto, K., and Harris, C. C. (2009) ING proteins as potential anticancer drug targets. *Current Drug Targets* **10,** 442–454
23. Dignam, J. D., Lebovitz, R. M., and Roeder, R. G. (1983) Accurate transcription initiation by RNA polymerase II in a soluble extract from isolated mammalian nuclei. *Nucleic Acids Res.* **11,** 1475–1489
24. Washburn, M. P., Wolters, D., and Yates, J. R., 3rd (2001) Large-scale analysis of the yeast proteome by multidimensional protein identification technology. *Nat. Biotechnol.* **19,** 242–247
25. Wolters, D. A., Washburn, M. P., and Yates, J. R., 3rd (2001) An automated multidimensional protein identification technology for shotgun proteomics. *Anal. Chem.* **73,** 5683–5690
26. McDonald, W. H., Ohi, R., Miyamoto, D. T., Mitchison, T. J., and Yates, J. R. (2002) Comparison of three directly coupled HPLC MS/MS strategies for identification of proteins from complex mixtures: single-dimension LCMS/MS, 2-phase MudPIT, and 3-phase MudPIT. *Int. J. Mass Spectrom.* **219,** 245–251
27. Florens, L., and Washburn, M. P. (2006) Proteomic analysis by multidimensional protein identification technology. *Methods Mol. Biol.* **328,** 159–175
28. Eng, J., McCormack, A. L., and Yates, J. R., III (1994) An approach to correlate tandem mass spectral data of peptides with amino acid sequences in a protein database. *J. Am. Mass Spectrom.* **5,** 976–989
29. Tabb, D. L., McDonald, W. H., and Yates, J. R., 3rd (2002) DTASelect and Contrast: tools for assembling and comparing protein identifications from shotgun proteomics. *J. Proteome Res.* **1,** 21–26
30. Zybailov, B., Mosley, A. L., Sardiu, M. E., Coleman, M. K., Florens, L., and Washburn, M. P. (2006) Statistical analysis of membrane proteome expression changes in Saccharomyces cerevisiae. *J. Proteome Res.* **5,** 2339–2347
31. Shannon, P., Markiel, A., Ozier, O., Baliga, N. S., Wang, J. T., Ramage, D., Amin, N., Schwikowski, B., and Ideker, T. (2003) Cytoscape: a software environment for integrated models of biomolecular interaction networks. *Genome Res.* **13,** 2498–2504
32. Irizarry, R. A., Hobbs, B., Collin, F., Beazer-Barclay, Y. D., Antonellis, K. J., Scherf, U., and Speed, T. P. (2003) Exploration, normalization, and summaries of high density oligonucleotide array probe level data. *Biostatistics* **4,** 249–264
33. Smyth, G. K. (2004) Linear models and empirical bayes methods for assessing differential expression in microarray experiments. *Stat. Appl. Genet. Mol. Biol.* **3,** Article 3
34. Benjamini, Y., and Hochber, Y. (1995) Controlling the false discovery rate: a practical and powerful approach to multiple testing. *J. Roy. Stat. Soc. B* **57,** 289–300
35. Söding, J., Biegert, A., and Lupas, A. N. (2005) The HHpred interactive server for protein homology detection and structure prediction. *Nucleic Acids Res.* **33,** W244–248
36. Mosley, A. L., Florens, L., Wen, Z., and Washburn, M. P. (2009) A label free quantitative proteomic analysis of the Saccharomyces cerevisiae nucleus. *J. Proteomics* **72,** 110–120
37. Zhang, Y., Wen, Z., Washburn, M. P., and Florens, L. (2010) Refinements to label free proteome quantitation: how to deal with peptides shared by multiple proteins. *Anal. Chem.* **82,** 2272–2281
38. Mosley, A. L., Sardiu, M. E., Pattenden, S. G., Workman, J. L., Florens, L., and Washburn, M. P. (2011) Highly reproducible label free quantitative proteomic analysis of RNA polymerase complexes. *Mol. Cell. Proteomics* **10,** M110.000687
39. Shiio, Y., Rose, D. W., Aur, R., Donohoe, S., Aebersold, R., and Eisenman, R. N. (2006) Identification and characterization of SAP25, a novel component of the mSin3 corepressor complex. *Mol. Cell. Biol.* **26,** 1386–1397
40. Katz, E., Dubois-Marshall, S., Sims, A. H., Gautier, P., Caldwell, H., Meehan, R. R., and Harrison, D. J. (2011) An in vitro model that recapitulates the epithelial to mesenchymal transition (EMT) in human breast cancer. *PLoS One* **6,** e17083
41. Shi, X., Hong, T., Walter, K. L., Ewalt, M., Michishita, E., Hung, T., Carney, D., Pena, P., Lan, F., Kaadige, M. R., Lacoste, N., Cayrou, C., Davrazou, F., Saha, A., Cairns, B. R., Ayer, D. E., Kutateladze, T. G., Shi, Y., Côté, J., Chua, K. F., and Gozani, O. (2006) ING2 PHD domain links histone H3 lysine 4 methylation to active gene repression. *Nature* **442,** 96–99
42. Egeblad, M., Rasch, M. G., and Weaver, V. M. (2010) Dynamic interplay between the collagen scaffold and tumor evolution. *Current Opinion Cell Biol.* **22,** 697–706
43. Zhang, Y., Handley, D., Kaplan, T., Yu, H., Bais, A. S., Richards, T., Pandit, K. V., Zeng, Q., Benos, P. V., Friedman, N., Eickelberg, O., and Kaminski, N. (2011) High throughput determination of TGFbeta1/SMAD3 targets in A549 lung epithelial cells. *PLoS One* **6,** e20319
44. Kiemer, A. K., Takeuchi, K., and Quinlan, M. P. (2001) Identification of genes involved in epithelial-mesenchymal transition and tumor progression. *Oncogene* **20,** 6679–6688
45. Lee, E. K., Han, G. Y., Park, H. W., Song, Y. J., and Kim, C. W. (2010) Transgelin promotes migration and invasion of cancer stem cells. *J. Proteome Res.* **9,** 5108–5117
46. Yu, H., Königshoff, M., Jayachandran, A., Handley, D., Seeger, W., Kaminski, N., and Eickelberg, O. (2008) Transgelin is a direct target of TGF-beta/Smad3-dependent epithelial cell migration in lung fibrosis. *FASEB J.* **22,** 1778–1789
47. Micalizzi, D. S., Farabaugh, S. M., and Ford, H. L. (2010) Epithelial-mesenchymal transition in cancer: parallels between normal development and tumor progression. *J. Mammary Gland Biol. Neoplasia* **15,** 117–134
48. Halder, S. K., Beauchamp, R. D., and Datta, P. K. (2005) A specific inhibitor of TGF-beta receptor kinase, SB-431542, as a potent antitumor agent for human cancers. *Neoplasia* **7,** 509–521
49. Keshamouni, V. G., Michailidis, G., Grasso, C. S., Anthwal, S., Strahler, J. R., Walker, A., Arenberg, D. A., Reddy, R. C., Akulapalli, S., Thannickal, V. J., Standiford, T. J., Andrews, P. C., and Omenn, G. S. (2006) Differential protein expression profiling by iTRAQ-2DLC-MS/MS of lung cancer cells undergoing epithelial-mesenchymal transition reveals a migratory/invasive phenotype. *J. Proteome Res.* **5,** 1143–1154
50. Hjelmeland, M. D., Hjelmeland, A. B., Sathornsumetee, S., Reese, E. D., Herbstreith, M. H., Laping, N. J., Friedman, H. S., Bigner, D. D., Wang, X. F., and Rich, J. N. (2004) SB-431542, a small molecule transforming growth factor-beta-receptor antagonist, inhibits human glioma cell line proliferation and motility. *Mol. Cancer Ther.* **3,** 737–745
51. Markowitz, S., Wang, J., Myeroff, L., Parsons, R., Sun, L., Lutterbaugh, J., Fan, R. S., Zborowska, E., Kinzler, K. W., Vogelstein, B., *et al.* (1995) Inactivation of the type II TGF-beta receptor in colon cancer cells with microsatellite instability. *Science* **268,** 1336–1338
52. Miyafuji, Y., Zhong, X., Uchida, I., Koi, M., and Hemmi, H. (2001) Growth inhibition due to complementation of transforming growth factor-beta receptor type II-defect by human chromosome 3 transfer in human colorectal carcinoma cells. *J. Cell. Physiol.* **187,** 356–364
53. Munoz, I. M., Macartney, T., Sanchez-Pulido, L., Ponting, C. P., Rocha, S., and Rouse, J. (2012) FAM60A (Family with sequence similarity 60A) is a cell cycle-fluctuating regulator of the SIN3-HDAC1 histone deacetylase complex. *J. Biol. Chem.* **287,** 32346–32353
54. McDonel, P., Demmers, J., Tan, D. W., Watt, F., and Hendrich, B. D. (2012) Sin3a is essential for the genome integrity and viability of pluripotent cells. *Dev. Biol.* **363,** 62–73
55. Meulmeester, E., and Ten Dijke, P. (2011) The dynamic roles of TGF-beta in cancer. *J. Pathol.* **223,** 205–218
56. Margadant, C., and Sonnenberg, A. (2010) Integrin-TGF-beta crosstalk in fibrosis, cancer and wound healing. *EMBO Rep.* **11,** 97–105
57. Hurst, D. R., and Welch, D. R. (2011) Metastasis suppressor genes at the interface between the environment and tumor cell growth. *Int. Rev. Cell*

Mol. Biol. **286,** 107–180
58. Yoshikawa, M., Hishikawa, K., Marumo, T., and Fujita, T. (2007) Inhibition of histone deacetylase activity suppresses epithelial-to-mesenchymal transition induced by TGF-beta1 in human renal epithelial cells. *J. Am. Soc. Nephrol.* **18,** 58–65
59. Srivastava, R. K., Kurzrock, R., and Shankar, S. (2010) MS-275 sensitizes TRAIL-resistant breast cancer cells, inhibits angiogenesis and metastasis, and reverses epithelial-mesenchymal transition in vivo. *Mol. Cancer Ther.* **9,** 3254–3266
60. Lei, W., Zhang, K., Pan, X., Hu, Y., Wang, D., Yuan, X., Shu, G., and Song, J. (2010) Histone deacetylase 1 is required for transforming growth factor-beta1-induced epithelial-mesenchymal transition. *Int. J. Biochem. Cell Biol.* **42,** 1489–1497
61. Bruzzese, F., Leone, A., Rocco, M., Carbone, C., Piro, G., Caraglia, M., Di Gennaro, E., and Budillon, A. (2011) HDAC inhibitor vorinostat enhances the antitumor effect of gefitinib in squamous cell carcinoma of head and neck by modulating ErbB receptor expression and reverting EMT. *J. Cell. Physiol.* **226,** 2378–2390
62. Kumamoto, K., Fujita, K., Kurotani, R., Saito, M., Unoki, M., Hagiwara, N., Shiga, H., Bowman, E. D., Yanaihara, N., Okamura, S., Nagashima, M., Miyamoto, K., Takenoshita, S., Yokota, J., and Harris, C. C. (2009) ING2 is upregulated in colon cancer and increases invasion by enhanced MMP13 expression. *Int. J. Cancer* **125,** 1306–1315
63. Lai, A. Y., and Wade, P. A. (2011) Cancer biology and NuRD: a multifaceted chromatin remodelling complex. *Nat. Rev. Cancer* **11,** 588–596
64. Yu, Y., Zeng, P., Xiong, J., Liu, Z., Berger, S. L., and Merlino, G. (2010) Epigenetic drugs can stimulate metastasis through enhanced expression of the pro-metastatic Ezrin gene. *PLoS One* **5,** e12710
65. Fujita, N., Jaye, D. L., Kajita, M., Geigerman, C., Moreno, C. S., and Wade, P. A. (2003) MTA3, a Mi-2/NuRD complex subunit, regulates an invasive growth pathway in breast cancer. *Cell* **113,** 207–219
66. Salisbury, C. M., and Cravatt, B. F. (2007) Activity-based probes for proteomic profiling of histone deacetylase complexes. *Proc. Natl. Acad. Sci. U. S. A.* **104,** 1171–1176
67. Mahrour, N., Redwine, W. B., Florens, L., Swanson, S. K., Martin-Brown, S., Bradford, W. D., Staehling-Hampton, K., Washburn, M. P., Conaway, R. C., and Conaway, J. W. (2008) Characterization of Cullin-box sequences that direct recruitment of Cul2-Rbx1 and Cul5-Rbx2 modules to Elongin BC-based ubiquitin ligases. *J. Biol. Chem.* **283,** 8005–8013.
68. Petroziello, J., Yamane, A., Westendorf, L., Thompson, M., McDonagh, C., Cerveny, C., Law, C. L., Wahl, A., and Carter, P. (2004). Suppression subtractive hybridization and expression profiling identifies a unique set of genes overexpressed in non-small-cell lung cancer. *Oncogene.* **23,** 7734–7745